

Comparative study of ferromagnetism in non-Heisenberg 1/1 and 2/1 quasicrystal approximants

Farid Labib^{1,*}, Takafumi D. Yamamoto², Asuka Ishikawa¹ and Ryuji Tamura²

¹Research Institute of Science and Technology, Tokyo University of Science, Tokyo 125-8585, Japan

²Department of Materials Science and Technology, Tokyo University of Science, Tokyo 125-8585, Japan



(Received 21 October 2023; accepted 22 April 2024; published 16 May 2024)

We report comparative study of ferromagnetic properties in non-Heisenberg 1/1 and 2/1 approximant crystals (ACs) with close chemical compositions in the quinary Au-Cu-Al-In-Tb alloy system. The 1/1 and 2/1 ACs exhibit comparable Weiss temperatures [$\theta_w = +17.8(5)$ and $+14.6(5)$ K], Curie temperatures ($T_C = 15.8$ and 14.3 K), and magnetic entropy changes (ΔS_M) under 5 T magnetic field change (-3.8 and -3.7 J/K mol Tb), respectively, showing insignificant role of the AC degree in the magnetism of the non-Heisenberg ACs. Moreover, the magnetic behavior of the quinary 1/1 AC is almost identical to that of the ternary $\text{Au}_{64}\text{Al}_{22}\text{Tb}_{14}$ 1/1 AC [N. Kikugawa, *et al.*, *J. Alloys Compd.* **882**, 160669 (2021).], which implies that chemical disorder introduced in the quinary 1/1 AC does not appreciably affect the ferromagnetic behavior, pointing toward the dominant magnetic interactions on a shorter length scale. The comparable magnetic behaviors between the 1/1 and 2/1 ACs are partly understood in terms of the similar distribution profiles of the interspin distances, up to third-nearest neighbor interactions, well beyond the common icosahedral cluster.

DOI: [10.1103/PhysRevB.109.174429](https://doi.org/10.1103/PhysRevB.109.174429)

I. INTRODUCTION

Quasicrystals (QCs) are long-range ordered intermetallic compounds exhibiting nonperiodic array of Bragg reflections with fivefold rotational symmetry in their diffraction patterns [1,2]. Approximant crystals (AC), on the other hand, are closely related periodic phases to QCs that crystalize within cubic lattices sharing the same multishell polyhedron motif of icosahedral quasicrystals (iQCs) in their atomic structure, as depicted in Fig. 1(a) (a rhombic triacontahedron, RTH) in the case of Tsai-type systems. Despite lacking long-range aperiodic order, the atomic structure of the ACs is essentially identical to iQCs over a short-range scale of a common cluster. Figures 1(b) and 1(c) show schematic configuration of the RTH clusters together with calculated electron diffraction (ED) patterns along pseudo-fivefold [508] axes within unit cells of 1/1 and 2/1 ACs. Pseudo-tenfold symmetries of the strong reflections in both ED patterns (being more pronounced in the latter) reflect structural similarity of the 1/1 and 2/1 ACs to the iQC with icosahedral symmetry. The 2/1 AC, in particular, encompasses all the structural motifs of the iQC, i.e., RTH, acute rhombohedra (AR), and obtuse rhombohedra (OR), making it an ideal system for experimentally probing impacts of structural aperiodicity on physical properties.

Amongst various types of iQCs and ACs, Tsai-type variants stand out due to their intriguing physical properties including long-range ferromagnetic (FM) [3–10], antiferromagnetic (AFM) [11–17] orders, and an unconventional quantum critical phenomenon [18]. Their magnetic properties are believed to be governed by Ruderman-Kittel-Kasuya-Yosida (RKKY) indirect coupling between $4f$ electrons of the localized moments and the conduction electrons [19,20].

Strikingly, both FM and AFM 1/1 ACs showcase noncoplanar magnetic structures with spins whirling around the [111] axis [14,21–25]. Recently, magnetic entropy change (ΔS_M) in the FM $\text{Au}_{64}\text{Al}_{22}\text{RE}_{14}$ ($\text{RE} = \text{Gd}, \text{Tb}, \text{and Dy}$) 1/1 ACs has been studied [26] macroscopically and adverse effect of Ising-like single-ion anisotropy (e.g., in Tb- and Dy-contained ACs) on ΔS_M is reported. In Ref. [27], ΔS_M of the Au-Si-Gd 1/1 AC has been revealed to be almost identical to that of $\text{Au}_{64}\text{Al}_{22}\text{Gd}_{14}$ 1/1 AC.

Despite the above progress on magnetic properties of Tsai-type alloys, a central yet unsolved question remains whether structural complexity associated with approximation degrees of ACs (i.e., 1/1, 2/1, etc.) impacts long-range magnetic order. To date, no magnetically ordered 1/1 and 2/1 ACs (or iQC) are known to form in the same alloy system. Such compounds, if available, can provide a unique playground to address the above matter experimentally. Here, we report successful synthesis of not only same alloy system but compositionally close quinary Au-Cu-Al-In-Tb 1/1 and 2/1 ACs exhibiting FM long-range order. Compositional proximity condition is necessary to ensure that both ACs have close electron concentrations, characterized by electron per atom (e/a), which is believed to impact magnetic properties of the ACs via RKKY mechanism [28]. With five distinct alloying elements, the present quinary ACs exhibit higher chemical disorder than their ternary $\text{Au}_{64}\text{Al}_{22}\text{Tb}_{14}$ 1/1 AC mother alloy [26], providing further opportunity to probe the influence of chemical disorder in magnetism of Tsai-type compounds with identical e/a . Benefiting from such opportunities, we report comparative investigation of bulk magnetic properties including ΔS_M on FM 1/1 and 2/1 ACs, both with $e/a = 1.74$. The results are explained based on the detailed analyses of their interspin distance (r) distributions using structural models of the prototypes Cd_6Yb 1/1 AC [29] and $\text{Cd}_{76}\text{Yb}_{13}$ 2/1 AC [30]. The results suggested *insignificant* effects of chemical disorder

*Corresponding author: labib.farid@rs.tus.ac.jp

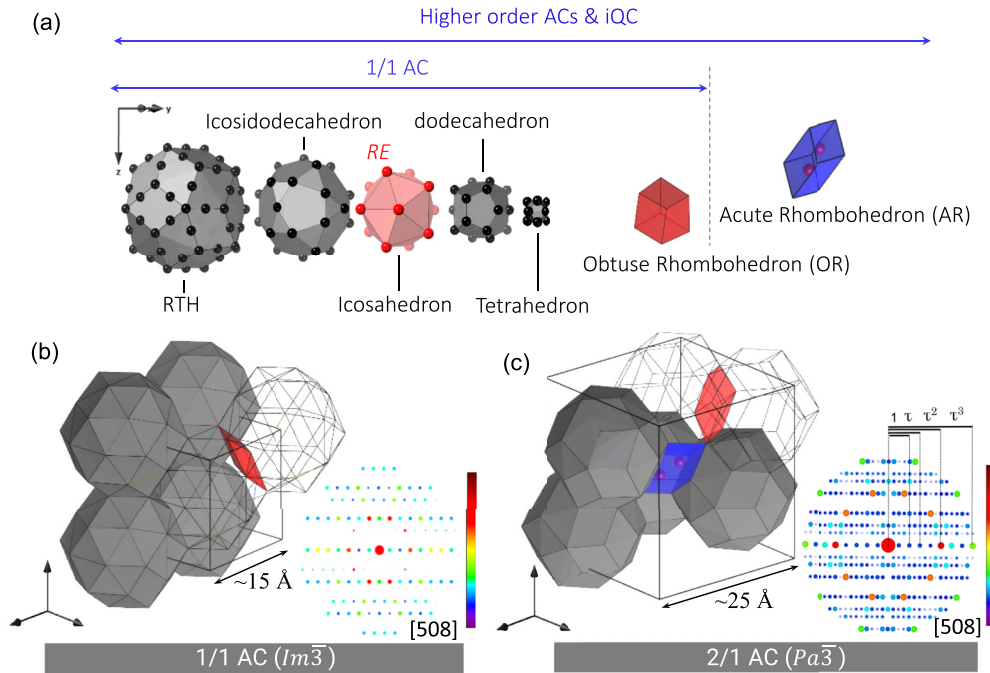


FIG. 1. (a) A typical shell structure of the Tsai-type *i*QC and ACs. From the outermost shell to the center: a rhombic triacontahedron (RTH) with 92 atoms sites, an icosidodecahedron (30 atomic sites), an icosahedron (12 atomic sites), a dodecahedron (20 atomic sites) and an innermost tetrahedron (4 atomic sites). Typical arrangement of RTH clusters within a unit cell of (b) 1/1 AC and (c) 2/1 AC. The latter include acute rhombohedra (AR) and obtuse rhombohedra (OR) units, which are also present in the *i*QC structure. To improve visibility, some RTH clusters are eliminated in the illustration. Beside each cluster configuration, corresponding calculated electron diffraction pattern along pseudo-fivefold [508] direction are provided. The color of the calculated diffraction spots indicates their intensity modulations. Despite their periodic nature, both patterns showcase pseudo-tenfold rotational symmetry in their diffraction patterns with the latter well imitating a tenfold symmetry inherent to QC structure.

and/or AC degree on magnetic properties of non-Heisenberg Tsai-type compounds.

II. EXPERIMENT

To prepare polycrystalline quinary 1/1 and 2/1 ACs, stoichiometric concentrations of monovalent Cu and trivalent In are added to the ternary $\text{Au}_{64}\text{Al}_{22}\text{Tb}_{14}$ 1/1 AC mother alloy [26] (following Hume-Rothery stability conditions [31]) resulting in quinary compounds with nearly identical e/a ratios of ~ 1.74 and effective chemical compositions of $\text{Au}_{56.4}\text{Al}_{10.8}\text{Cu}_{6.9}\text{In}_{11.8}\text{Tb}_{14.1}$ and $\text{Au}_{56.1}\text{Al}_{10.5}\text{Cu}_{6.9}\text{In}_{11.8}\text{Tb}_{14.7}$, respectively (refer to Fig. S1 in the Supplemental Material [32] for their corresponding backscattering scanning electron microscopy images). The arc-melting technique followed by 100 h of isothermal annealing at 773 and 673 K for the 1/1 and 2/1 ACs, respectively, was employed for synthesizing the alloys. Nearly 0.6 at. % higher concentration of Tb in the 2/1 AC is due to the presence of AR units in the atomic structure that incorporates additional RE elements along their long body-diagonal axis (see Fig. 1 for schematic illustration of AR unit within a unit cell). The reason for thermodynamic stabilization of the 2/1 AC from the ternary 1/1 AC mother alloy after iso-valent elemental substitution is unclear at the moment. We suspect that geometrical parameters correlated with atomic radius of the constituent elements may play a key role in switching AC degree from lower to higher. Using a similar ap-

proach, a search for *i*QC in the same alloy system is currently in progress.

For phase identification, powder x-ray diffraction (XRD) was employed using Rigaku SmartLab SE x-ray diffractometer with $\text{Cu-K}\alpha$ radiation. For microstructure observation, a scanning electron microscope (SEM), JEOL JSM-IT100 equipped with energy-dispersive x-ray spectrometer was utilized. For phase characterization, selected area electron diffraction (SAED) patterns were obtained using a transmission electron microscopy instrument JEM-2010F, located at the Advanced Research Infrastructure for Materials and Nanotechnology at the University of Tokyo. Superconducting quantum interference device magnetometer (Quantum Design, MPMS3) was utilized to examine the bulk magnetization under zero-field-cooled (ZFC) and field-cooled (FC) conditions within a temperature range of 1.8 K to 300 K and under external dc fields up to 7 T. Additionally, specific-heat measurements were conducted in a temperature range of 2–50 K by a thermal relaxation method using a Quantum Design physical property measurement system (PPMS). The ΔS_M was determined by analyzing a series of temperature-dependent magnetization (M vs T) curves under various magnetic fields within the temperature range of 2 to 120 K, employing a thermodynamic Maxwell relation.

III. RESULTS

Figure 2 displays powder XRD patterns of the synthesized 1/1 and 2/1 ACs, along with their Le Bail fittings. The fittings

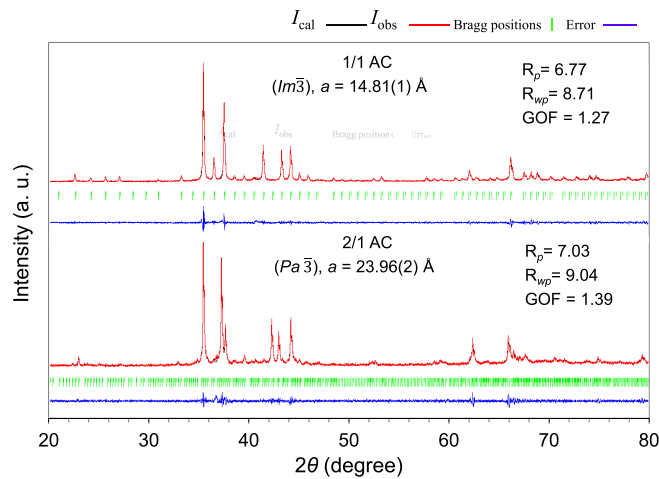


FIG. 2. Le Bail fitting of the powder XRD patterns of (a) 1/1 AC and (b) 2/1 AC. The observed (I_{obs}) and calculated (I_{cal}) peak intensities, the difference between the two, and the expected Bragg peak positions are represented by red, black, and blue lines and green bars, respectively. R_p , R_{wp} , and GOF are profile R factor, weighted-profile R factor, and goodness of fit defined as R_{wp}/R_{exp} , respectively.

were conducted using the JANA 2006 software suite [33], assuming the space groups $Im\bar{3}$ and $Pa\bar{3}$ for the 1/1 and 2/1 ACs, respectively. The red, black, and blue lines represent the observed (I_{obs}) and calculated (I_{cal}) peak intensities, and the difference between the two, respectively. The expected Bragg peak positions are indicated by the green bars. From the fittings, the lattice parameters of the 2/1 and 1/1 ACs were determined to be 23.92(2) and 14.80(3) Å, respectively. The excellent agreement between the calculated and experimental peaks in Fig. 2 confirms the high quality of the synthesized samples, making them suitable for further analysis of their physical properties.

Figure 3 showcases SAED patterns obtained from incidence axes perpendicular to (a), (b) [110] and (c), (d) [111] directions of the (a), (c) 1/1 AC and (b), (d) 2/1 AC. The patterns are consistent with the cubic symmetries and space groups $Im\bar{3}$ and $Pa\bar{3}$ for the 1/1 and 2/1 ACs, respectively, validating the Le Bail fitting results in Fig. 2 where these conditions are applied. In addition, no superlattice reflections were observed in the SAED patterns. Furthermore, in Figs. 3(c) and 3(d), clear zigzag arrangement of the diffraction spots is observed. In principle, ACs can be viewed as QCs with “linear phason strain” [34], the magnitude of which can be gauged from disposition of the strong reflections from ideal positions observed in strain-free iQC. The zigzag configuration of the reflections in Figs. 3(c) and 3(d) (being insignificant in the latter) is a direct evidence of “linear phason strain” in ACs [35,36]. Therefore, from x-ray and ED patterns in Figs. 2 and 3, the present quinary 1/1 and 2/1 ACs are regarded as cubic ACs isostructural to Cd_6Yb 1/1 AC [29] and $Cd_{76}Yb_{13}$ 2/1 AC [30] prototypes with space groups $Im\bar{3}$ and $Pa\bar{3}$, respectively.

In Fig. S2 in the Supplemental Material [32], the high-temperature inverse magnetic susceptibility (H/M) of the compounds is presented within a temperature range of 1.8–300 K. The results demonstrate a linear behavior in

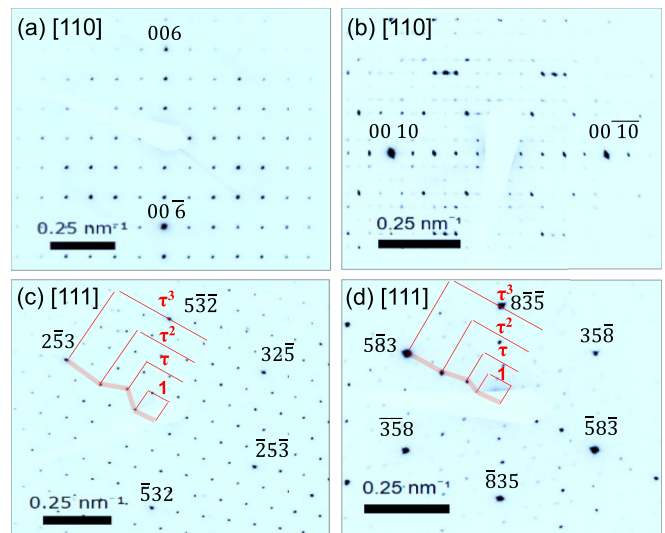


FIG. 3. SAED patterns obtained from (a), (c) 1/1 AC and (b,d) 2/1 AC along incident axes perpendicular to (a), (b) [110] and (c), (d) [111] directions. Zigzag configuration of the reflections in (c) and (d) reflects structural deviation of the ACs from a perfect aperiodic atomic arrangement in iQC and is denoted as “linear phason strain” in their structure.

both ACs, fitting well to the Curie-Weiss law: $M/H(T) = N_A \mu_{\text{eff}}^2 \mu_B^2 / 3k(T - \theta_w) + \chi_0$, where N_A , μ_{eff} , μ_B , k , θ_w , and χ_0 denote the Avogadro number, effective magnetic moment, Bohr magneton, Boltzmann constant, Curie-Weiss temperature, and the temperature-independent magnetic susceptibility, respectively. By extrapolating a linear least-squares fitting within a temperature range of 100 K $< T <$ 300 K, the estimated θ_w values of +17.8(5) and +14.6(5) K are derived for the 1/1 and 2/1 ACs, respectively, with χ_0 approximating to zero. The μ_{eff} values of both ACs are within a range of 9.57–9.71 μ_B , close to 9.72 μ_B , i.e., the calculated value for free Tb^{3+} ions defined as $g_J[J(J+1)]^{0.5} \mu_B$ [37], indicating the localization of magnetic moments on Tb^{3+} ions.

The temperature dependence of the dc magnetic susceptibility (M/H) of the 1/1 and 2/1 ACs is illustrated in Fig. 4 within the temperature range of 1.8–30 K under FC (filled circles) and ZFC (unfilled circles) modes. Both 1/1 and 2/1 ACs exhibit relatively sharp rise of their magnetic susceptibility below $T_C = 15.9$ and 14.2 K, respectively, which is attributed to the onset of spontaneous magnetization (M_s) following $M_s(T) = M_0(-\epsilon)^\beta$, where M_0 , ϵ , and β represent a critical amplitude, a reduced temperature $(T - T_C)/T_C$, and a critical exponent, respectively [refer to Fig. S6 and Eq. (1) in the Supplemental Material [32] for details]. The inset of Fig. 4 provides field-dependent magnetization curves ($M-H$) of the ACs at 1.8 K, demonstrating magnetization rise with magnetic field in both ACs reaching approximately $6\mu_B/Tb^{3+}$ (about 75% of the total moment of a free Tb^{3+} ion) at 7 T. The unsaturation to a full moment of Tb^{3+} at high magnetic fields is a common feature among ferromagnetically ordered non-Heisenberg ACs and is attributed to a strong uniaxial anisotropy of the spins with nonzero orbital angular momentum, as described elsewhere [5,38]. Both 1/1 and 2/1 ACs exhibit hysteresis loops at low magnetic fields (see Fig. S3

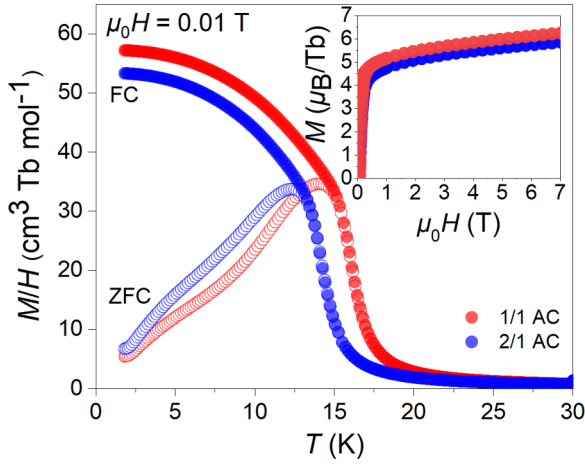


FIG. 4. Low-temperature magnetic susceptibility M/H of the 1/1 AC (represented by red) and 2/1 AC (represented by blue) under field-cooled (FC) and zero-field-cooled (ZFC) modes. The inset shows field-dependence magnetizations at 1.8 K up to $\mu_0 H = 7$ T.

in the Supplemental Material [32]) with the latter being slightly thinner, which might originate from their different domain sizes.

The temperature dependence of the specific heat divided by temperature (C_p/T) for the 1/1 AC (a red line) and 2/1 AC (a blue line), as well as the nonmagnetic $\text{Au}_{56.2}\text{Al}_{9.8}\text{Cu}_{6.7}\text{In}_{12.8}\text{Y}_{14.5}$ 2/1 AC (analyzed composition) within a temperature range of 1.8 – 50 K is provided in Fig. 5. The positions of pronounced anomalies at $T = 15.8$ and 14.3 K are in perfect agreement with the T_C values estimated from the magnetization data, confirming the establishment of long-range order in the studied ACs. In the paramagnetic region (above T_C), the C_p/T curves of the ACs overlap with each other, indicating nearly identical lattice contributions to C_p in lower- and higher-order ACs. The inset of Fig. 5 displays the magnetic entropy of the ACs with the error bars

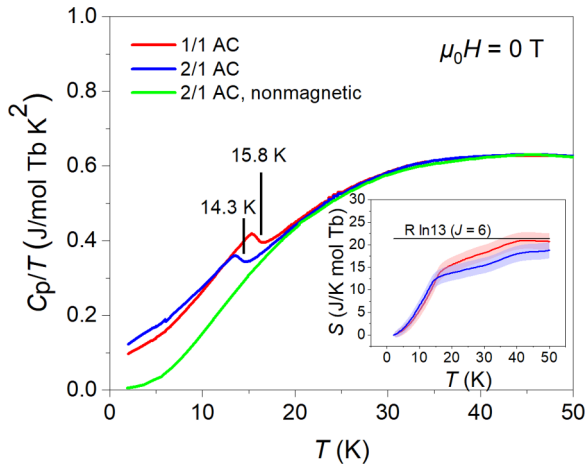


FIG. 5. The temperature dependence of the specific heat divided by temperature C_p/T for 1/1 AC (represented by red), 2/1 AC (blue), and nonmagnetic $\text{Au}_{56}\text{Al}_{10}\text{Cu}_7\text{In}_{13}\text{Y}_{14}$ 2/1 AC (green). The inset shows the magnetic entropy with the shaded area representing the error bar.

stemming from measured weight of the samples. The magnetic entropy in the samples has been estimated from the magnetic contribution to heat capacity (C_M), derived by subtracting the nonmagnetic (C_{NM}) contribution using the data of the $\text{Au}_{56.2}\text{Al}_{9.8}\text{Cu}_{6.7}\text{In}_{12.8}\text{Y}_{14.5}$ 2/1 AC and the following relation:

$$S_M = \int_0^T C_M/T dT. \quad (1)$$

Clearly, in both ACs, a zero-field magnetic entropy S_M approaches $R \ln(2J + 1)$, where J represents the total angular momentum ($J = 6$ for Tb^{3+}), which is the maximum magnetic entropy expected per mole of Tb^{3+} with R being a universal gas constant.

These results confirm the establishment of long-range FM order in the present 1/1 and 2/1 ACs. Due to the absence of a negative slope and/or an inflection point in the H/M versus M^2 curves shown in Fig. S4 in the Supplemental Material [32], phase transitions in both ACs can be characterized as second order (following Banerjee's criterion [39]). Further analyses based on the scaling principle and Kouvel-Fisher equations (refer to Supplemental Material [32] and Figs. S5-S7 therein for the details) reveal critical exponents of $(\beta; \gamma)$ of (0.40, 0.90) and (0.39, 1.08) for the 1/1 and 2/1 ACs, respectively, indicating a mean-field-like nature of the FM transition near T_C for both ACs. These values accord well with the $(\beta, \gamma) = (0.54, 0.89)$ [10] and (0.47, 1.12) [27] obtained from bulk magnetization data in Au-Ga-Dy *i*QC and Au-Si-Gd 1/1 AC, respectively, and $\beta = 0.44(2)$ [22] and $\beta = 0.56(4)$ [21] estimated from neutron-diffraction experiment in the $\text{Au}_{70}\text{Al}_{16}\text{Tb}_{14}$ and $\text{Au}_{65}\text{Ga}_{21}\text{Tb}_{14}$ 1/1 ACs, respectively.

Moving forward, we investigate magnetic entropy change (ΔS_M) of the present ACs around their transition temperatures. Figure 6 provides series of temperature dependence of the FC magnetization curves for (a) 1/1 AC and (b) 2/1 AC within a temperature range of 1.8–120 K and magnetic fields spanning from 0.01–7 T. The $-\Delta S_M$ variation with temperature for the 1/1 and 2/1 ACs [presented in Figs. 6(c) and 6(d), respectively] is estimated using the thermodynamic Maxwell relation [40]:

$$\Delta S_M(T, \Delta H) = \mu_0 \int_0^{H_{\max}} \left(\frac{\partial M(T, H)}{\partial T} \right)_H dH, \quad (2)$$

with M and H representing the magnetization and the external magnetic field, respectively. In both ACs, ΔS_M shows maximum around T_C reaching -3.8 and -3.7 J/K mol Tb in the 1/1 and 2/1 AC, respectively, under $\mu_0 \Delta H = 5$ T (or -4.3 and -4.1 J/K mol Tb, respectively, under $\mu_0 \Delta H = 7$ T). From Figs. 6(c) and 6(d), relative cooling power (RCP), which is a measure of heat transfer between the hot and cold reservoirs, can be estimated using the following equation [40]:

$$\text{RCP} = -\Delta S_M \times \delta T_{\text{FWHM}}, \quad (3)$$

where ΔS_M and δT_{FWHM} correspond to the maximum magnetic entropy change at given magnetic field and the full width at half maximum (FWHM) of the corresponding $\Delta S_M(T)$ curve, respectively. Table I lists estimated T_C , $-\Delta S_M$, and RCP values of the present ACs under $\mu_0 \Delta H = 5$ T, together with those reported for the $\text{Au}_{64}\text{Al}_{22}\text{RE}_{14}$ ($\text{RE} = \text{Gd}, \text{Tb}, \text{Dy}$)

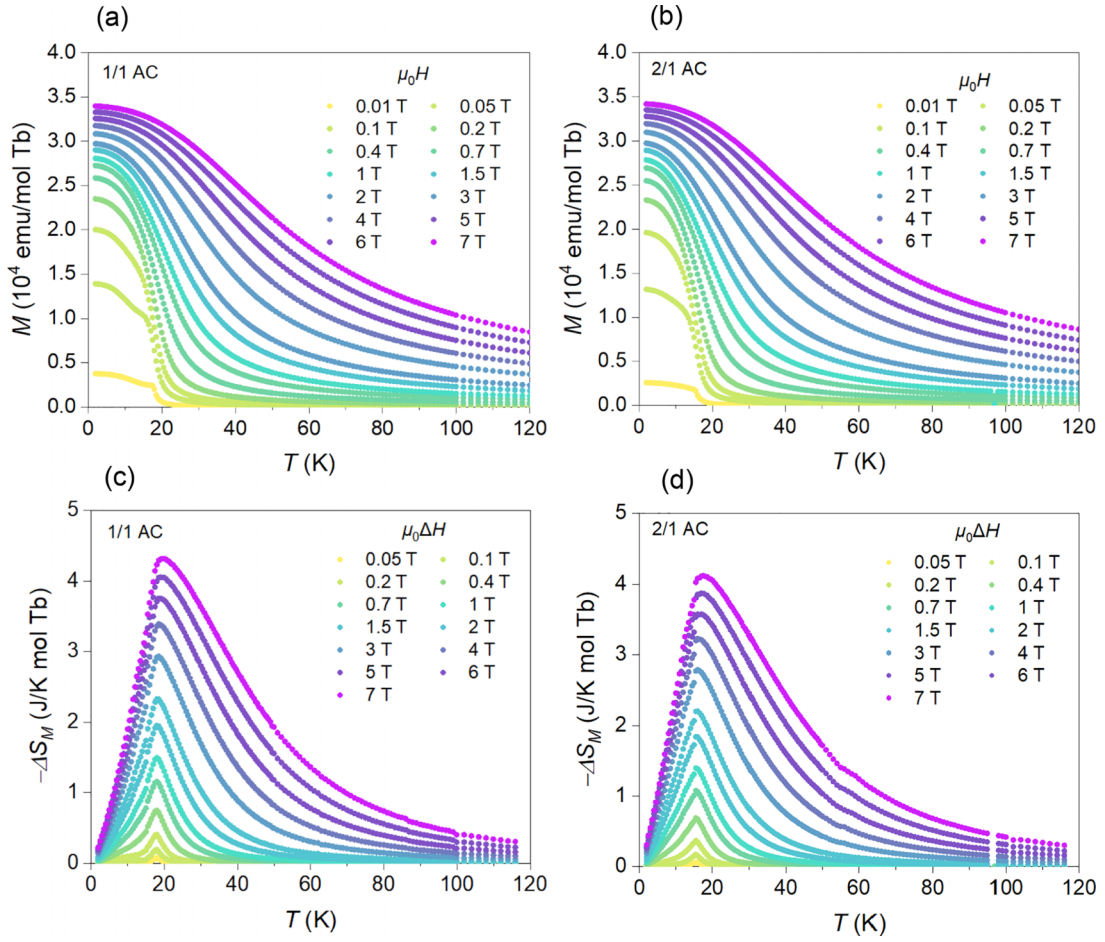


FIG. 6. Series of temperature dependence of magnetization under FC mode for (a) 1/1 AC, and (b) 2/1 AC under magnetic field spanning from 0.01–7 T. The corresponding ΔS_M are shown in (c) for 1/1 AC and (d) for 2/1 AC.

[26] and Au-Si-Gd [27] 1/1 ACs for the comparison. The results indicate nearly identical ΔS_M values for the Tb-contained ACs regardless of the alloy system being ternary or quinary and/or AC degree being 1/1 or 2/1.

Figure 7 positions the θ_w/dG of the present ACs [dG denotes de Gennes parameter expressed as $(g_J - 1)^2 J(J + 1)$, with g_J and J being the Landé g factor and the total angular momentum] within a wider universal framework of (θ_w/dG vs e/a) unique to Tsai-type compounds [28] (only Tb-contained compounds are shown). A solid oscillating curve corresponds to a third-order polynomial fitting to all data. Such oscillatory behavior of θ_w/dG with e/a is solid experimental evidence that indicates the domination of RKKY exchange interaction in

magnetic behavior of Tsai-type compounds. From Fig. 7, it is apparent that first, the θ_w/dG values of the present quinary ACs are nearly identical to that of ternary Au-Al-Tb 1/1 AC mother alloy (distinguished by a green triangular symbol) implying an *insignificant* effect of chemical disorder between the constituent elements on net magnetization of the non-Heisenberg Tsai-type compounds (θ_w represents net magnetic interaction on each spin). Notice that chemical disorder should shorten the RKKY interaction transmission range by introducing nonperiodic scattering centers for the potential wave [41]. Similar θ_w/dG values in the ternary and quinary ACs indicate that their net magnetization is not affected by the cut of RKKY transmission range, suggesting short-range nature

TABLE I. Comparison of the T_C , ΔS_M , and RCP under $\mu_0 \Delta H = 5$ T in the present ACs and previous reports.

AC type	Composition	T_C (K)	$-\Delta S_M$ (J/K mol Tb)	RCP (J/mol Tb)	Reference
1/1	Au _{56.4} Al _{10.8} Cu _{6.9} In _{11.8} Tb _{14.1}	15.9	3.8	115	This work
2/1	Au _{56.1} Al _{10.5} Cu _{6.9} In _{11.8} Tb _{14.7}	14.3	3.7	107	This work
1/1	Au ₆₄ Al ₂₂ Gd ₁₄	27	5.3	135	[26]
1/1	Au ₆₄ Al ₂₂ Tb ₁₄	15	3.9	105	[26]
1/1	Au ₆₄ Al ₂₂ Dy ₁₄	9.5	4.3	107	[26]
1/1	Au _{72.7} Si _{13.6} Gd _{13.7}	16.9	5.4	130	[27]

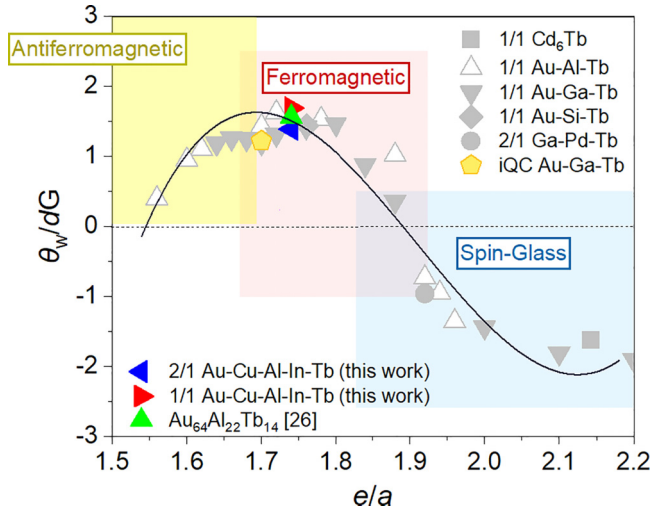


FIG. 7. Variation of normalized Weiss temperature θ_w/dG and the magnetic ground states vs the electron-per-atom (e/a) ratio spanning from 1.5 to 2.2 for the Tb-contained Tsai-type compounds including the present quinary 1/1 and 2/1 ACs. The oscillatory behavior of the polynomial fitting to the θ_w/dG is a universal behavior in Tsai-type compounds.

of the magnetic interactions in Tsai-type compounds. Second, the θ_w/dG values of the present ACs with $e/a \sim 1.74$ fall close together near a maximum of the fitting curve where strong FM interaction is expected. Interestingly, even Au-Ga-Tb iQC with e/a of 1.70 [8] (represented by a yellow pentagon symbol in Fig. 7) appears on the same curve close to the present ACs. This indicates dominant (respectively, marginal) effect of e/a (respectively, AC degree) on net magnetization of the Tsai-type compounds. In addition, close θ_w/dG values of the present 1/1 and 2/1 ACs suggests that the difference in their electronic structures is not significant as far as the magnetic properties are concerned (otherwise, the two ACs would show different θ_w and different e/a dependences).

Given that the magnetic interaction in the Tsai-type systems is majorly governed by RKKY mechanism [19,20], to clarify the above argument it is helpful to explore RKKY interaction energy which oscillates as $f(x) = (-x \cos x + \sin x)/x^4$; $x = 2k_F r$, where k_F is a Fermi wave number (assuming a spherical Fermi surface of radius k_F) and r is the interspin distance. In the following discussion, we analyze the r distributions in the 1/1 and 2/1 ACs using structural models of the prototypes Cd_6Yb 1/1 AC [29] and $Cd_{76}Yb_{13}$ 2/1 AC [30].

Figures 8(a) and 8(b) project spatial configurations of the RE elements within unit cells of the 1/1 and 2/1 ACs, respectively, along the pseudo-fivefold $[8\ 0\ 13]$ axis. In Fig. 8(c),

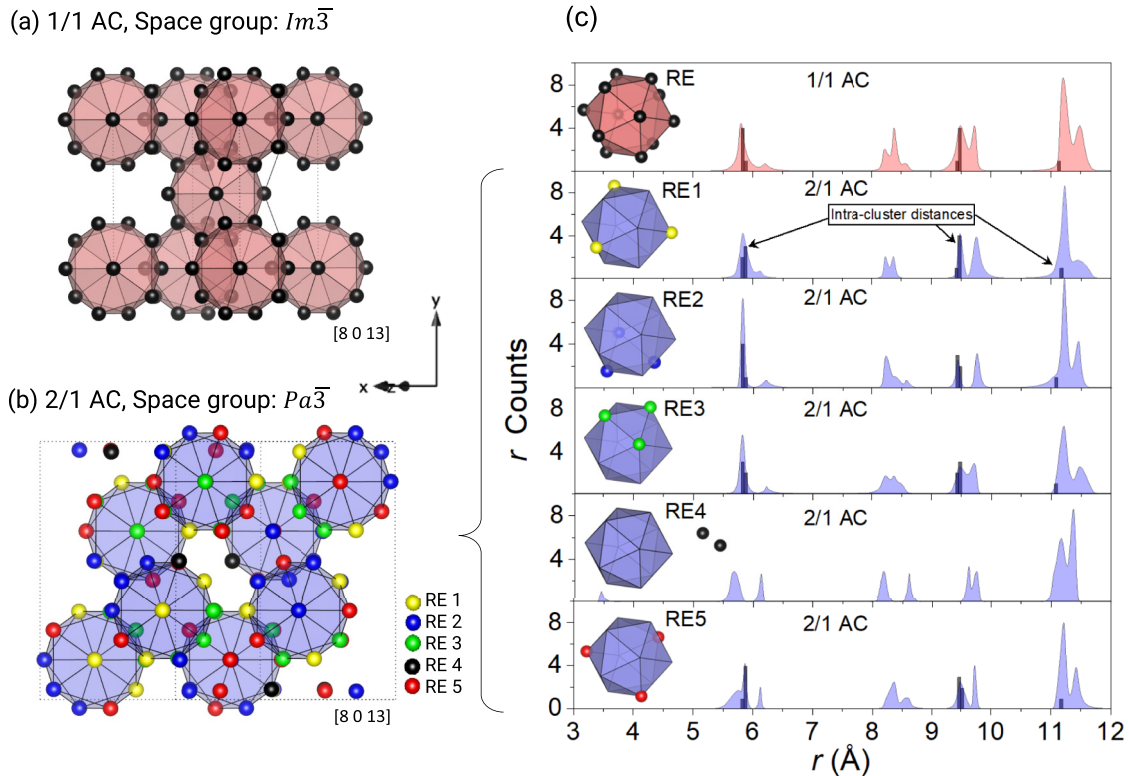


FIG. 8. Configuration of the RE elements on the icosahedron clusters in (a) 1/1 AC and (b) 2/1 AC. Different RE colors in (b) represents five distinct symmetrically inequivalent sites in the 2/1 AC. (c) represents r distribution in the 1/1 and 2/1 ACs within a range of 3 – 12 Å covering three-nearest neighbor interactions range. In the 2/1 AC, the r calculations are performed separately by setting each of the RE 1 – RE 5 atoms at the origin and measuring their distances from surrounding RE atoms up to 12 Å. In (c), duplicate distances have been removed and the bin size is set to 0.05 Å. The upper panel in (c) shows r distributions in the 1/1 AC and the lower panels represent those of RE 1 – RE 5 atoms in the 2/1 AC. The black bars in (c) show r distribution within a single icosahedron composed of 12 moments (denoted as intraplate distances; 11 distinct distances).

Gaussian distributions of $RE - RE$ distances are compared between the two ACs within a distance range of 3–12 Å covering three-nearest neighbor interactions. It should be emphasized that despite the 1/1 AC wherein all RE atoms are symmetrically equivalent, the 2/1 AC contains five distinct symmetrically inequivalent RE sites [represented by spheres of different colors in Fig. 8(b)] [15,42], with $RE1 - RE3$ and $RE5$ locating on the icosahedron vertices and the $RE4$ occupying positions inside the AR units [see Fig. 1 and Fig. 8(b)]. Owing to existence of REs with multiple crystallographic symmetries in the 2/1 AC, the r calculations are carried out by individually setting each of the five RE sites as the origin and systematically measuring the distances to all surrounding RE atoms (regardless of their symmetry) up to a radius of 12 Å. The upper panel of Fig. 8(c) corresponds to r distribution in the 1/1 AC and the bottom panels belong to $RE1 - RE5$ in the 2/1 ACs. The black bars with a bin size of 0.05 Å represent 11 distinct intracluster distances (i.e., distances within a single icosahedron cluster composed of only 12 moments), while colored Gaussian distributions represent all r distributions incorporating both intra- and intercluster (i.e., distances between REs located at the adjacent clusters).

What stands out in Fig. 8(c) is that despite their long-range structural dissimilarities, the 1/1 and 2/1 ACs exhibit strikingly similar r distribution profiles that extend well beyond the common icosahedral cluster (up to the third-nearest neighbor interactions). Even more interestingly is that the r distribution remains nearly robust against differences in RE site symmetries in the 2/1 AC, in particular $RE1 - RE3$ and $RE5$ that occupy icosahedron vertices. This implies that within the RKKY mechanism framework, we should not expect appreciable differences in exchange-coupling energies between the 1/1 and 2/1 AC as long as their electron concentrations (or e/a) remain close (which is the case for the present ACs). This conjecture, which is well supported by the experimental observations shown in Fig. 7, provides convincing structural evidence for the comparative magnetic behavior of not only the present 1/1 and 2/1 ACs, but also a large variety of Tsai-type compounds studied to date, regardless of their AC degree, constituent elements or perhaps structural aperiodicity (in the light of structural proximity between 2/1 AC and iQC).

From the present results, we further conclude that switching between AC degrees is not an effective approach in tuning the ΔS_M near T_C in Tsai-type compounds. To date, the e/a parameter remains the most powerful tool for that purpose.

IV. CONCLUSION

This study reports the synthesis and comparative investigation of magnetic properties, including magnetic entropy change (ΔS_M), for non-Heisenberg Tsai-type 1/1 and 2/1 approximant crystals (ACs) with nearly identical electron per atom (e/a) of 1.74 within the same quinary Au-Cu-Al-In-Tb system. The 1/1 and 2/1 ACs exhibit comparable Weiss temperatures (θ_w), Curie temperatures (T_C), and ΔS_M values, which also match closely with those reported for the ternary $Au_{64}Al_{22}Tb_{14}$ 1/1 AC [26]. This implies that varying the AC degree and chemical disorder has minimal impact on the magnetic behavior of non-Heisenberg Tsai-type compounds when the e/a ratio is held constant. Such insensitivity to chemical disorder highlights a substantial role of magnetic interactions on a shorter length scale in Tsai-type compounds. In fact, detailed analysis of the interspin distances (r) in the 1/1 and 2/1 ACs reveals very similar distributions, up to third-nearest neighbor interactions, far beyond the common icosahedral cluster. Thus, the present work provides an important basis for deeper understanding of the intrinsic magnetism of Tsai-type compounds including quasicrystals (QCs).

ACKNOWLEDGMENTS

The authors acknowledge Dr. Akiko. T. Saito at Magnetic and Spintronic Materials Research Center, National Institute for Materials Science (NIMS), Japan, for the heat-capacity measurements and thank Akiko Takeda for the assistance in the synthesis of the materials. This work was supported by Japan Society for the Promotion of Science through Grants-in-Aid for Scientific Research (Grants No. JP19H05817, No. JP19H05818, No. JP21H01044, and No. JP24K17016) and Japan Science and Technology agency, CREST, Japan, through Grant No. JPMJCR2203.

-
- [1] D. Shechtman, I. Blech, D. Gratias, and J. W. Cahn, Metallic phase with long-range orientational order and no translational symmetry, *Phys. Rev. Lett.* **53**, 1951 (1984).
 - [2] M. Duneau and A. Katz, Quasiperiodic patterns, *Phys. Rev. Lett.* **54**, 2688 (1985).
 - [3] K. Inagaki, S. Suzuki, A. Ishikawa, T. Tsugawa, F. Aya, T. Yamada, K. Tokiwa, T. Takeuchi, and R. Tamura, Ferromagnetic 2/1 quasicrystal approximants, *Phys. Rev. B* **101**, 180405(R) (2020).
 - [4] A. Ishikawa, T. Hiroto, K. Tokiwa, T. Fujii, and R. Tamura, Composition-driven spin glass to ferromagnetic transition in the quasicrystal approximant Au-Al-Gd, *Phys. Rev. B* **93**, 024416 (2016).
 - [5] T. Hiroto, K. Tokiwa, and R. Tamura, Sign of canted ferromagnetism in the quasicrystal approximants Au-SM-R (SM = Si, Ge and Sn/R = Tb, Dy and Ho), *J. Phys.: Condens. Matter* **26**, 216004 (2014).
 - [6] G. Gebresenbut, M. S. Andersson, P. Beran, P. Manuel, P. Nordblad, M. Sahlberg, and C. P. Gomez, Long range ordered magnetic and atomic structures of the quasicrystal approximant in the Tb-Au-Si system, *J. Phys.: Condens. Matter* **26**, 322202 (2014).
 - [7] T. Hiroto, G. H. Gebresenbut, C. Pay Gómez, Y. Muro, M. Isobe, Y. Ueda, K. Tokiwa, and R. Tamura, Ferromagnetism and re-entrant spin-glass transition in quasicrystal approximants Au-SM-Gd (SM = Si, Ge), *J. Phys.: Condens. Matter* **25**, 426004 (2013).
 - [8] R. Tamura, A. Ishikawa, S. Suzuki, A. Kotajima, Y. Tanaka, T. Seki, N. Shibata, T. Yamada, T. Fujii, C.-W. Wang, M. Avdeev, K. Nawa, D. Okuyama, and T. J. Sato, Experimental observation of long-range magnetic order in icosahedral quasicrystals, *J. Am. Chem. Soc.* **143**, 19928 (2021).
 - [9] F. Labib, S. Suzuki, A. Ishikawa, T. Fujii, and R. Tamura, Emergence of long-range magnetic order from spin-glass

- state by tuning electron density in a stoichiometric Ga-based quasicrystal approximant, *Phys. Rev. B* **106**, 174436 (2022).
- [10] R. Takeuchi, F. Labib, T. Tsugawa, Y. Akai, A. Ishikawa, S. Suzuki, T. Fujii, and R. Tamura, High phase-purity and composition-tunable ferromagnetic icosahedral quasicrystal, *Phys. Rev. Lett.* **130**, 176701 (2023).
- [11] R. Tamura, Y. Muro, T. Hiroto, K. Nishimoto, and T. Takabatake, Long-range magnetic order in the quasicrystalline approximant Cd₆Tb, *Phys. Rev. B* **82**, 220201(R) (2010).
- [12] D. H. Ryan, J. M. Cadogan, T. Kong, P. C. Canfield, A. I. Goldman, and A. Kreyssig, A neutron diffraction demonstration of long-range magnetic order in the quasicrystal approximant DyCd₆, *AIP Adv.* **9**, 035312 (2019).
- [13] A. Ishikawa, T. Fujii, T. Takeuchi, T. Yamada, Y. Matsushita, and R. Tamura, Antiferromagnetic order is possible in ternary quasicrystal approximants, *Phys. Rev. B* **98**, 220403(R) (2018).
- [14] T. J. Sato, A. Ishikawa, A. Sakurai, M. Hattori, M. Avdeev, and R. Tamura, Whirling spin order in the quasicrystal approximant Au₇₂Al₁₄Tb₁₄, *Phys. Rev. B* **100**, 054417 (2019).
- [15] F. Labib, H. Takakura, A. Ishikawa, and R. Tamura, Atomic structure of the unique antiferromagnetic 2/1 quasicrystal approximant, *Phys. Rev. B* **107**, 184110 (2023).
- [16] S. Yoshida, S. Suzuki, T. Yamada, T. Fujii, A. Ishikawa, and R. Tamura, Antiferromagnetic order survives in the higher-order quasicrystal approximant, *Phys. Rev. B* **100**, 180409(R) (2019).
- [17] F. Labib, D. Okuyama, N. Fujita, T. Yamada, S. Ohhashi, D. Morikawa, K. Tsuda, T. J. Sato, and A. P. Tsai, Structural transition-driven antiferromagnetic to spin-glass transition in Cd-Mg-Tb 1/1 approximants, *J. Phys.: Condens. Matter* **32**, 485801 (2020).
- [18] K. Deguchi, S. Matsukawa, N. K. Sato, T. Hattori, K. Ishida, H. Takakura, and T. Ishimasa, Quantum critical state in a magnetic quasicrystal, *Nat. Mater.* **11**, 1013 (2012).
- [19] S. Watanabe, Magnetism and topology in Tb-based icosahedral quasicrystal, *Sci. Rep.* **11**, 1 (2021).
- [20] S. Thiem and J. T. Chalker, Magnetism in rare-earth quasicrystals: RKKY interactions and ordering, *EPL* **110**, 17002 (2015).
- [21] K. Nawa, M. Avdeev, A. Ishikawa, H. Takakura, C.-W. Wang, D. Okuyama, R. Murasaki, R. Tamura, and T. J. Sato, Magnetic properties of the quasicrystal approximant Au₆₅Ga₂₁Tb₁₄, *Phys. Rev. Mater.* **7**, 054412 (2023).
- [22] K. Nawa, D. Okuyama, A. Ebina, T. J. Sato, A. Ishikawa, and R. Tamura, Single-crystal neutron diffraction study on the quasicrystal approximant Au₇₀Al₁₆Tb₁₄, *J. Phys. Conf. Ser.* **2461**, 012015 (2023).
- [23] T. Hiroto, T. J. Sato, H. Cao, T. Hawaii, T. Yokoo, S. Itoh, and R. Tamura, Noncoplanar ferrimagnetism and local crystalline-electric-field anisotropy in the quasicrystal approximant Au₇₀Si₁₇Tb₁₃, *J. Phys. Condens. Matter* **32**, 415802 (2020).
- [24] G. H. Gebresenbut *et al.*, Effect of pseudo-Tsai cluster incorporation on the magnetic structures of R-Au-Si (R = Tb, Ho) quasicrystal approximants, *Phys. Rev. B* **106**, 184413 (2022).
- [25] F. Labib, K. Nawa, S. Suzuki, H. Wu, A. Ishikawa, K. Inagaki, T. Fujii, T. J. Sato, and R. Tamura, Unveiling exotic magnetic phase diagram of a non-Heisenberg quasicrystal approximant, *Mater. Today Phys.* **40**, 101321 (2024).
- [26] N. Kikugawa, T. Hiroto, A. Ishikawa, S. Suzuki, H. Sakurai, and R. Tamura, Magnetocaloric effect in ferromagnetic 1/1 quasicrystal approximants Au₆₄Al₂₂R₁₄ (R = Gd, Tb, and Dy), *J. Alloys Compd.* **882**, 160669 (2021).
- [27] T. Shiino, G. H. Gebresenbut, C. P. Gómez, U. Häussermann, P. Nordblad, A. Rydh, and R. Mathieu, Examination of the critical behavior and magnetocaloric effect of the ferromagnetic Gd-Au-Si quasicrystal approximants, *Phys. Rev. B* **106**, 174405 (2022).
- [28] S. Suzuki, A. Ishikawa, T. Yamada, T. Sugimoto, A. Sakurai, and R. Tamura, Magnetism of Tsai-type quasicrystal approximants, *Mater. Trans.* **62**, 298 (2021).
- [29] C. P. Gómez and S. Lidin, Comparative structural study of the disordered MCd₆ quasicrystal approximants, *Phys. Rev. B* **68**, 024203 (2003).
- [30] C. P. Gomez and S. Lidin, Structure of Ca₁₃Cd₇₆: A novel approximant to the MCd_{5,7} quasicrystals (M = Ca, Yb), *Angew. Chem. Int. Ed.* **40**, 4037 (2001).
- [31] T. Fujiwara and Y. Ishii, *Quasicrystals. Handbook of Metal Physics*, 1st ed. (Elsevier, Amsterdam, 2008).
- [32] See Supplemental Material at <http://link.aps.org/supplemental/10.1103/PhysRevB.109.174429> for the backscattering electron images; high-temperature inverse magnetic susceptibility; field-dependence magnetization loops at low magnetic fields; Arrott plots and detailed analyses of critical behavior of the present 1/1 and 2/1 approximant crystals based on scaling principle and Kouvel-Fisher equations. The Supplemental Material also contains Ref. [39].
- [33] V. Petříček, M. Dušek, and L. Palatinus, Crystallographic computing system JANA2006: General features, *Zeitschrift für Krist. - Cryst. Mater.* **229**, 345 (2014).
- [34] Z. M. Stadnik, *Physical Properties of Quasicrystals* (Springer, Berlin, 1998).
- [35] A. P. Tsai, Discovery of stable icosahedral quasicrystals: Progress in understanding structure and properties, *Chem. Soc. Rev.* **42**, 5352 (2013).
- [36] A. P. Tsai, Icosahedral clusters, icosahedral order and stability of quasicrystals—A view of metallurgy, *Sci. Technol. Adv. Mater.* **9**, 013008 (2008).
- [37] S. Blundell, *Magnetism in Condensed Matter Physics*, 1st ed. (Oxford University Press, New York, 2001).
- [38] G. H. Gebresenbut, M. S. Andersson, P. Nordblad, M. Sahlberg, and C. Pay Gómez, Tailoring magnetic behavior in the Tb-Au-Si quasicrystal approximant system, *Inorg. Chem.* **55**, 2001 (2016).
- [39] M. Parra-Borderías, F. Bartolomé, J. Herrero-Albillos, and L. M. García, Detailed discrimination of the order of magnetic transitions and magnetocaloric effect in pure and pseudobinary Co Laves phases, *J. Alloys Compd.* **481**, 48 (2009).
- [40] A. M. Tishin and Y. I. Spichkin, *The Magnetocaloric Effects and Its Applications* (IOP Publishing, Bristol and Philadelphia, 2003).
- [41] A. J. Heeger, A. P. Klein, and P. Tu, Effect of mean free path on the Ruderman-Kittel-Kasuya-Yoshida spin-density oscillations, *Phys. Rev. Lett.* **17**, 803 (1966).
- [42] T. Yamada, Superstructure formation in a ternary Yb-Cd-Mg 1/1 quasicrystal approximant, *Philos. Mag.* **101**, 257 (2021).